ELSEVIER

Journal of Power Sources 68 (1997) 686–691

JOURNAL OF POWER SOURCES

Structure and charge/discharge characteristics of new layered oxides: $Li_{1.8}Ru_{0.6}Fe_{0.6}O_3$ and Li_2IrO_3

Hironori Kobayashi [a,*], Ryoji Kanno [b], Mitsuharu Tabuchi [a], Hiroyuki Kageyama [a], Osamu Nakamura [a], Mikio Takano [c]

[a] *Osaka National Research Institute, AIST, MITI, 1-8-31 Midorigaoka, Ikeda, Osaka 563, Japan*

[b] *Department of Chemistry, Faculty of Science, Kobe University, Nada, Kobe, Hyogo 657, Japan*

[c] *Institute for Chemical Research, Kyoto University, Uji, Kyoto 611, Japan*

Accepted 13 November 1996

Abstract

New layered oxides, $Li_2(Ru_{1-y}Fe_y)O_3$ and Li_2IrO_3, were synthesized and characterized by X-ray diffractometry, Mössbauer spectroscopy and electrochemical measurements. In the $Li_2(Ru_{1-y}Fe_y)O_3$ system, symmetry change from a monoclinic to a rhombohedral structure was observed near $y=0.4$ with increasing iron content, y, from 0 to 0.5. The rhombohedral monophase obtained at $y=0.5$ has the composition of $Li_{1.8}Ru_{0.6}Fe_{0.6}O_3$ with the layered α-$NaFeO_2$-type structure. Li_2IrO_3 has rhombohedral symmetry with the Li_2RuO_3-related structure. Lithium cells using $Li_{1.8}Ru_{0.6}Fe_{0.6}O_3$ and Li_2IrO_3 cathodes showed cycling capacities of 100 and 120 mAh/g, respectively. © 1997 Published by Elsevier Science S.A

Keywords: Lithium de-intercalation; Layered oxides; Ruthenium oxide; Iridium oxide

1. Introduction

Layered oxides Li_2MO_3 (M = Mn, Ti, Ru, Sn, Mo) have cubic-close packed oxide-ion lattices with basal planes of octahedral interstices filled alternately by Li^+ only and by $1/3Li^+$, $2/3M^{4+}$ [1–9]. Of these metal components, the $Ru^{5+/4+}$ and $Mo^{5+/4+}$ couples permit lithium extraction from the host structure [1,9–13]. Recently, we studied the structural changes with delithiation and electrochemical behavior in the $Li_{2-x}RuO_3$ system and found that the de-intercalation proceeded from $x=0.0$ to 1.3 and the Li/Li_2RuO_3 cells showed excellent reversibility in the voltage range, 3.0–4.0 V, with an energy density of 160 mAh/g [12,13].

Fig. 1 shows relationship between the ionic radii of metal ions and the lattice symmetry of Li_2MO_3. Rhombohedral phases are reported for M = Pt and Mo with $0.63 < r < 0.65$ Å. The structure of Li_2MoO_3 has a cationic ordering that 1/3 Li and 2/3 Mo distributes randomly in the $LiMo_2$ layers [9]. The monoclinic Li_2MO_3 (M = Ru, Sn, Zr) have different stacking of cation layers along the

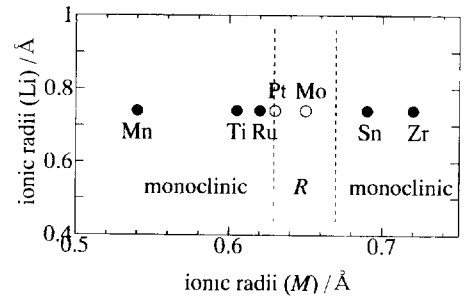

Fig. 1. Relationship between ionic radius (M) and lattice symmetry of Li_2MO_3. *R* represents rhombohedral symmetry.

c-axis [1,7,8]; in Li_2RuO_3, the Ru^{4+} hexagonal networks in successive $LiRu_2$ layers are displaced by (0, 1/2, 1/2) in lattice coordinates. Difference in the symmetry is related to the cationic ordering of Li and M ions, which is explained either by the electronic structure [1] or the size factors of M^{4+} ions [7]. To date, Li_2IrO_3 has not been reported where the ionic radius of Ir^{4+} ($r=0.63$ Å) is equal to that of Pt^{4+} ($r=0.63$ Å) [14]. We are interested in the synthesis and characterization of Li_2IrO_3. If a layered phase Li_2IrO_3 exists, the structure might give us a useful

* Corresponding author

PII S0378-7753(96)02597-9

information on the factor which determines the structural varieties in Li_2MO_3 compounds. Another approach to clarify the structural differences is that of a substitution of different cations into the structure, for example, a substitution of Ru for Fe in Li_2RuO_3. Furthermore, the charge/discharge cycle performance might give us information on the diffusion of Li ion in Li_2MO_3 compounds.

In the present study, we synthesized the $Li_2(Ru_{1-y}Fe_y)O_3$ system and clarified the new layered phase, $Li_{1.8}Ru_{0.6}Fe_{0.6}O_3$. We also synthesized a new layered oxide Li_2IrO_3. Electrochemical properties of $Li_{1.8}Ru_{0.6}Fe_{0.6}O_3$ and Li_2IrO_3 were investigated and the relationship between the structures and the electrochemical properties is discussed.

2. Experimental

The quaternary oxides $Li_2(Ru_{1-y}Fe_y)O_3$ and ternary oxide Li_2IrO_3 were prepared by heating appropriate molar ratios of Li_2CO_3, RuO_2, IrO_2, and Fe_3O_4 (Li_2CO_3 and Fe_3O_4: Nakarai Chemicals, >99.0% purity; RuO_2, IrO_2: Furuuchi Chemicals, >99.99% purity). These samples were predried, mixed and pelletized; $Li_2(Ru_{1-y}Fe_y)O_3$ was fired in air or under oxygen gas flow at 1073–1373 K for 24–64 h, and Li_2IrO_3 was fired in air at 923–1323 K for 24–48 h.

X-ray diffraction (XRD) patterns of the powdered samples were obtained with an X-ray diffractometer (Rigaku RAD-C) with Cu Kα radiation. The XRD data were collected for 3–6 s at each 0.04° step width over a 2θ range from 15 to 120°. The structural parameters were refined by Rietveld analysis using the computer program RIETAN [15].

Electrochemical intercalation and de-intercalation were carried out using lithium cells. The working electrode consisted of a mixture of 50–100 mg samples, 10–20 mg acetylene black and 0.3 mg Teflon powder pressed into a tablet of 13 mm diameter under a pressure of 9 MPa. The cells used for the electrochemical tests were constructed in a stainless-steel 2016 coin-type configuration (20 mm outside diameter and 1.6 mm thickness). The counter electrode was a 15 mm diameter and 0.24 mm thickness disk of lithium metal foil. The separator employed was a microporous polypropylene sheet. Two typical electrolytes (Mitsubishi Petrochemical Company, battery grade) were used in these cells: (i) 1 M solutions of $LiClO_4$ in a 50:50 mixture of propylene carbonate (PC) and 1,2 dimethoxyethane (DME) by volume, and (ii) 1 M solutions of $LiClO_4$ in a 50:50 mixture of PC and 1,2 dimethoxycarbonate (DMC). The PC:DME electrolyte was used for cells with a cell voltage of lower than 4.4 V and the PC:DMC electrolyte was used for cells with a cell voltage of lower than 4.8 V. The cells were constructed in an argon-filled glove-box. The current density was calculated based on the cathode area. The electrochemical measurements were carried out at room temperature after standing overnight under zero current flow. Cell properties were measured galvanostatically.

Mössbauer spectra was measured at room temperature by using Mössbauer spectroscopy apparatus (ELSINT). The velocity was corrected by pure Fe as the standard materials. The data were computer-fitted assuming a hyperfine component made of absorption peaks of the Lorentzian line shape.

3. Results and discussion

3.1. $Li_2(Ru_{1-y}Fe_y)O_3$

3.1.1. Synthesis

Fig. 2 shows the XRD patterns for $Li_2(Ru_{1-y}Fe_y)O_3$ synthesized under an oxygen gas flow at 1273 K for 24 h. Nominal compositions are indicated in the figure. The XRD peaks of $35° < 2\theta < 39°$ and $19° < 2\theta < 23°$ are shown in Fig. 2(b) and (c), respectively. The peaks in Fig. 2(b) shift continuously with increasing Fe content. The peaks indexed as 020 and $11\bar{1}$ reflections, which are characteristic for the monoclinic phase shift at $0 \le y \le 0.3$. However, the intensity of these peaks decreased at $y = 0.4$ and disappeared at $y = 0.5$. At $y = 0.5$, all the XRD peaks could be indexed by a pseudo-hexagonal lattice similar to that of α-$NaFeO_2$. In order to distinguish the two-phase and single-

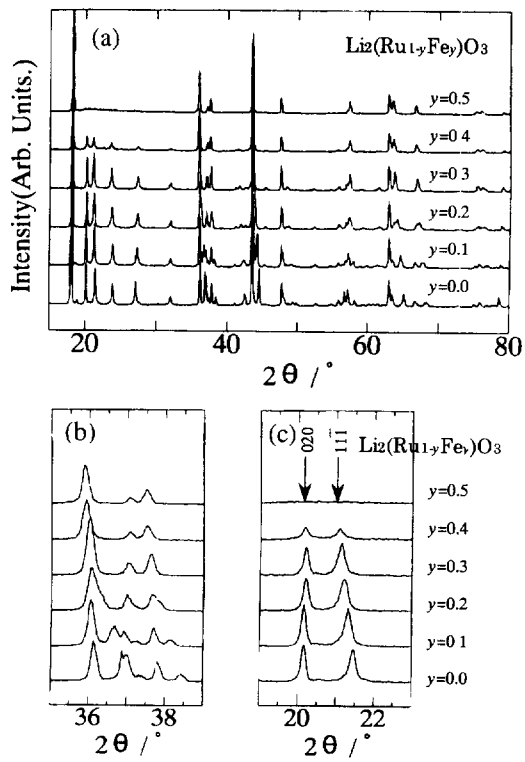

Fig. 2. XRD patterns for $Li_2(Ru_{1-y}Fe_y)O_3$ synthesized under an oxygen gas flow at 1273 K for 24 h. Nominal compositions are indicated in the figure.

Table 1
Lattice parameters for $Li_2(Ru_{1-y}Fe_y)O_3$; lattice parameters were refined using single-phase model for $0<y<0.3$ and $y=0.5$, and using two-phase model for $y=0.4$. Monoclinic and pseudo-hexagonal cells were represented by 'm' and 'h', respectively

Composition	a	b	c	β	R_{wp}	R_e
a) *single-phase model*						
$y=0.0$ (m)	4.9230(3)	8.7746(5)	9.8776(6)	100.073(4)	From Ref. [12]	
$y=0.1$ (m)	4.9692(2)	8.7843(5)	9.8667(5)	100.024(4)	18.91	6.07
$y=0.2$ (m)	5.0168(3)	8.7594(6)	9.8491(6)	99.900(5)	17.88	5.85
$y=0.3$ (m)	5.0569(5)	8.7712(7)	9.8491(6)	99.832(9)	17.61	6.84
b) *two-phase model*						
$y=0.4$ (m)	5.0706(8)	8.7758(12)	9.8429(14)	99.794(14)	11.69	6.69
$y=0.4$ (h)	2.9194(2)		14.4769(12)			
c) *single-phase model*						
$y=0.5$ (h)	2.9302(15)		14.540(5)		11.59	6.36

phase regions in $0<y<0.5$, the lattice parameters were refined using XRD data. At $y=0.4$, the refinement using a single-phase model led to a slightly higher R value. Table 1 lists final R factor and lattice parameters, and their estimated standard deviations. Fig. 3 shows the composition dependence of the lattice parameters for $Li_2(Ru_{1-y}Fe_y)O_3$. Lattice parameters of the monoclinic phases are transformed to a pseudo-hexagonal unit cell with the relation as follows: $a_h \sim (1/\sqrt{3})a_m$, $b_h \sim (1/3)b_m$, and $c_h \sim [(3/2)\sin\beta] \times c_m$, where the subscripts, 'h' and 'm', are used to represent the pseudo-hexagonal and monoclinic cells, respectively. In the monoclinic phases, the a-axis parameter increases and the b- and c- axis parameters decrease with increasing y from 0.0 to 0.3. No significant difference was observed between the a-xis and b-axis parameters at $y=0.4$. At $y=0.5$, relative peak intensity ratios $I(003)$ against the other peaks in the pseudo-hexagonal unit cell increased with increasing synthesis temperature from 1123 to 1273 K and remained constant between 1273 and 1323 K. The samples started to decompose above 1373 K and decomposed completely at 1473 K. The new phase at $y=0.5$ in $Li_2(Ru_{1-y}Fe_y)O_3$, was thus synthesized in air at a reaction temperature of 1323 K for 48 h.

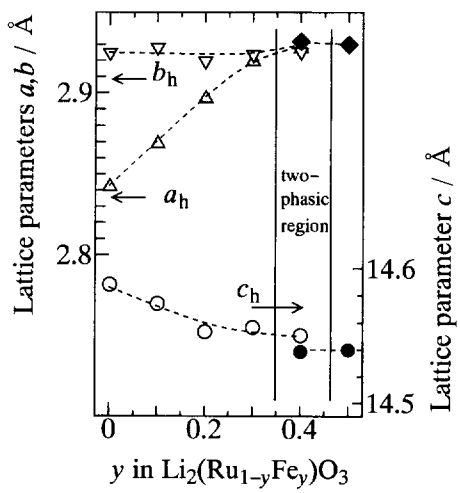

Fig. 3. Composition dependence of the lattice parameters for $Li_2(Ru_{1-y}Fe_y)O_3$.

The Li:Ru:Fe ratio of the new phase was determined by inductively coupled plasma (ICP) emission spectrometry. Alkali fusion method was used as pre-treatment for the samples. The ratio was determined to be 2.78:1.0:1.0. Mössbauer spectra measurement showed that the profile shape of the spectra and the parameter for the isomer shift (0.350 mm/s) are both characteristic for Fe^{3+} ions in the oxides. We analyzed the composition of this compound by ICP emission spectrometry and Mössbauer spectroscopy. These results suggested the composition $Li_{1.74}Ru_{0.63}Fe_{0.63}O_3$ when no defect in the cation/anion site exist; the error limit of our chemical analysis might be 0.03. Here the valence state of Ru ion included partially Ru^{3+}. Because Ru^{3+} was a slightly unusual valence state, we indicated in the manuscript that the valence state of Ru ion was Ru^{4+}. Therefore, the composition was determined to be $Li_{1.8}Ru_{0.6}Fe_{0.6}O_3$ where Ru and Fe ions are in 4+ and 3+ valence states, respectively.

3.1.2. Structure

The XRD pattern was indexed by a pseudo-hexagonal cell with $a=2.9302(6)$ Å, $c=14.5395(4)$ Å. The structure was refined with space group $R\bar{3}m$ using a structural model of Li_2MoO_3 [9]. Ru at 3*b* (0.0, 0.0, 0.5), Fe(1) at 3*b* (0.0, 0.0, 0.5), Li(1) at 3*b* (0.0, 0.0, 0.5), Fe(2) at 3*a* (0.0, 0.0, 0.0), Li(2) at 3*a* (0.0, 0.0, 0.0), O at 6*c* (0.0, 0.0, z) with $z=\sim 0.25$. Disordered arrangements of Ru, Fe(1) and Li(1) at the 3*b* sites and Fe(2) and Li(2) at the 3*a* sites were considered with the constraint that the

Table 2
Structural parameters for $Li_{1.8}Ru_{0.6}Fe_{0.6}O_3$ in $R\bar{3}m$

$a = 2.9302(6)$ Å, $c = 14.5395(4)$ Å, $B = 0.8(3)$ Å^2, $R_{wp} = 11.59$ %, $R_e = 6.37$%, $R_I = 4.60$ %					
Atom	Site	g	x	y	z
Ru	3*b*	0.4	0.0	0.0	0.5
Fe(1)	3*b*	0.362(17)	0.0	0.0	0.5
Li(1)	3*b*	0.238	0.0	0.0	0.5
Fe(2)	3*a*	0.038	0.0	0.0	0.0
Li(2)	3*a*	0.962	0.0	0.0	0.0
O	6*c*	1.0	0.0	0.0	0.2446(17)

total occupancy is unity at each sites. The site occupation parameters, g, of Fe(1), Fe(2), Li(1), and Li(2) sites were refined. The refinement using a structural model that the Fe ions exist in the 3*a* site led to a slightly lower R value. The B's for all sites were constrained to be the same value. No correction was made for preferred orientation. Table 2 lists final R factor, lattice and structural parameters, and their estimated standard deviations. The compositions of Li_2MoO_3 and $Li_{1.8}Ru_{0.6}Fe_{0.6}O_3$ could be expressed as $(Li)_{3a}(Mo_{0.667}Li_{0.333})_{3b}O_2$ and $(Li_{0.962}Fe_{0.038})_{3a}(Ru_{0.4}Fe_{0.362}Li_{0.238})_{3b}O_2$, respectively. The structural difference in the both structures is the cation arrangement at 3*a* site: the octahedral 3*a* sites are occupied by Li^+ only in Li_2MoO_3, while these sites are occupied by both Li^+ and a small amount of Fe^{3+} in $Li_{1.8}Ru_{0.6}Fe_{0.6}O_3$.

3.1.3. Electrochemical properties

De-intercalation experiments were carried out using the cells $Li/Li_{1.8}Ru_{0.6}Fe_{0.6}O_3$ with PC:DME electrolytes. Fig. 4 shows the constant charge curves of the cells as a function of x in $Li_{1.8-x}Ru_{0.6}Fe_{0.6}O_3$. The current densities are shown in the figure. The extraction of lithium from $Li_{1.8}Ru_{0.6}Fe_{0.6}O_3$ proceeded from $x = 0$ to $x = 1.3$ with a single-phase reaction which is indicated by the continuously increased discharge curve from 3.5 to 4.3 V. The curve showed a slope change around $x = 0.4$, which suggests a change in the de-intercalation mechanism. The charge capacity decreased with increasing current density.

Reversibility of the $Li/Li_{1.8}Ru_{0.6}Fe_{0.6}O_3$ cells was examined in the voltage range, 2.0–4.3 V, with a current density of 0.1 mA/cm^2. Fig. 5 shows the charge and discharge curves. The charge capacity for the first cycle was 240 mAh/g, and 120 mAh/g for the second cycle. Capacity loss was observed after the first cycle, and then no degradation was found with cycling. The loss could be caused by a decomposition of the PC:DME electrolytes or a decomposition of the layered structure of $Li_{1.8}Ru_{0.6}Fe_{0.6}O_3$ after the first charge cycle. To examine the effect of electrolyte, de-intercalation experiments were carried out using cells $Li/Li_{1.8}Ru_{0.6}Fe_{0.6}O_3$ with PC:DMC electrolytes. However, no significant difference was found when

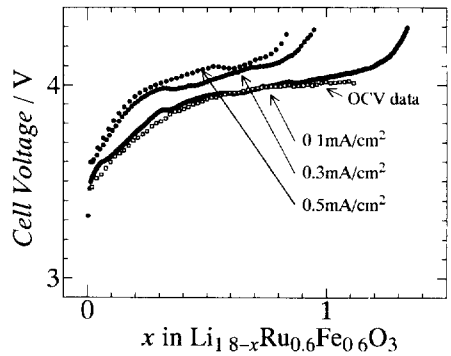

Fig. 4. The constant charge curves of the cell, $Li/Li_{1.8}Ru_{0.6}Fe_{0.6}O_3$, with a current density of 0.1, 0.3 and 0.5 mA/cm^2 together with the quasi OCV curve with 0.1 mA/cm^2

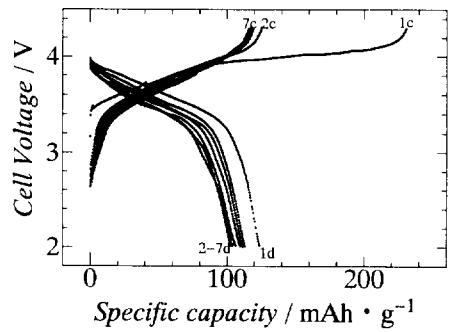

Fig. 5. Charge and discharge curves of the cell, $Li/Li_{1.8}Ru_{0.6}Fe_{0.6}O_3$, with a current density of 0.1 mA/cm^2 and cut-off voltages of 2.0 and 4.3 V

the PC:DME and PC:DMC electrolyte were used for the cells.

Mössbauer spectra measured for $Li_{1.8-x}Ru_{0.6}Fe_{0.6}O_3$ ($x = 0.6$) indicated the isomer shift (0.308 mm/s), which is characteristics for the Fe^{3+} state; XRD patterns of the sample during the first charge process indicated a monophasic reaction, which corresponds to a change in oxidation state from Ru^{4+} to Ru^{6+}. However, Ru^{6+} is not a realistic valence state of ruthenium ions. It is therefore reasonable that the lithium de-intercalation was caused by the valence change from Ru^{4+} to Ru^{5+}. The amount of

lithium extraction $x = \sim 0.6$ might be consistent with the reversible discharge/charge capacity of 120 mAh/g ($0 \leq x \leq 0.6$). Further study based on chemical extraction might be necessary to clarify the mechanism of the first charge process.

3.2. Li_2IrO_3

3.2.1. Synthesis

Fig. 6 shows the XRD pattern for Li_2IrO_3 synthesized in air at 1223 K for 48 h. The XRD patterns are different from those with orthorhombic symmetry reported by Gadzhiev and Shaplygin [16]. All of the XRD peaks could be indexed by a pseudo-hexagonal cell with $a = 5.1687(12)$ Å, $c = 14.461(8)$ Å. The XRD pattern of Li_2IrO_3 shows characteristics peaks corresponding to these of Ru^{4+} hexagonal networks in Li_2RuO_3. This suggests that Ir^{4+} hexagonal network exists in $LiIr_2$ layers. Detailed structural analysis of the new phase is currently in progress.

3.2.2. Electrochemical properties

De-intercalation experiments were carried out using the cells Li/Li_2IrO_3 with PC:DME electrolytes. The extraction of lithium proceeded from $x = 0$ to $x = 1.5$ in $Li_{2-x}IrO_3$ with potential plateaus around 3.5 V ($0 < x < 0.8$) and 4.2 V ($1.2 < x < 1.4$). Reversibility of the Li/Li_2IrO_3 cells was examined in the voltage range, 2.0–4.4 V, with the current density of 0.2 mA/cm^2. Fig. 7 shows the charge and discharge curves. No significant degradation was observed for the charge/discharge curves after the second cycle with energy densities of 120 mAh/g and a low overpotential for the electrode process.

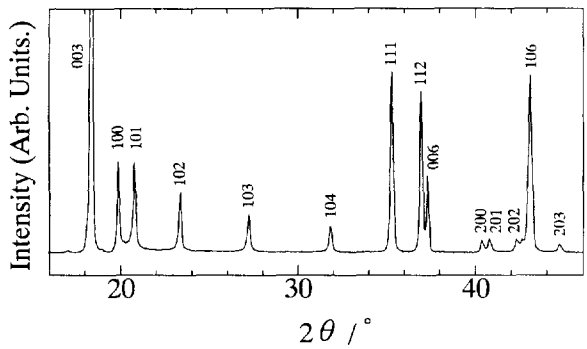

Fig. 6. XRD pattern for Li_2IrO_3 synthesized in air at 1223 K for 48 h. The *hkl* indexed by the pseudo-hexagonal lattice are indicated in the figure.

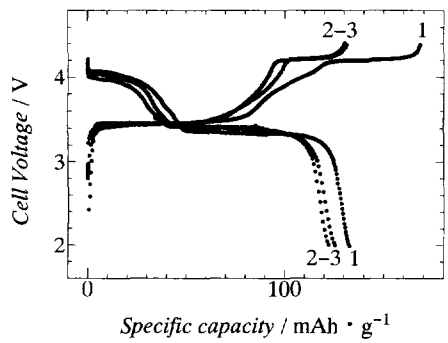

Fig. 7 Charge and discharge curves of the cell, Li/Li_2IrO_3, with a current density of 0.2 mA/cm^2 and cut-off voltages of 2.0 and 4.4 V

4. Conclusions

In the present study, the new layered oxides, $Li_{1.8}Ru_{0.6}Fe_{0.6}O_3$ and Li_2IrO_3, were synthesized. $Li_{1.8}Ru_{0.6}Fe_{0.6}O_3$ has the α-$NaFeO_2$ structure and Li_2IrO_3 has rhombohedral symmetry with the Li_2RuO_3-related structure. The change from monoclinic (Li_2RuO_3) to rhombohedral ($Li_{1.8}Ru_{0.6}Fe_{0.6}O_3$) was caused by the substitution for Ru^{4+} of Fe^{3+} ions, which indicated that the structures of Li_2MO_3 compounds are primarily dependent on the size factor of M cations. The new oxide $Li_{1.8}Ru_{0.6}Fe_{0.6}O_3$ has rhombohedral symmetry with the Li_2MoO_3-type. The average ionic radius of 0.6325 Å for ($Ru_{0.6}Fe_{0.6}$) [Ru^{4+} ($r = 0.62$ Å) and Fe^{3+} ($r = 0.645$ Å)] is situated in the region, 0.63 Å (Pt^{4+}) $< r <$ 0.65 Å (Mo^{4+}), where the rhombohedral structure is stable (see Fig. 1). The lithium cells consisted of $Li/Li_{1.8}Ru_{0.6}Fe_{0.6}O_3$ and Li/Li_2IrO_3 couple showed reversibility in the voltage range, 2.0–4.3 V, and an energy density of 100 and 120 mAh/g, respectively.

Acknowledgements

This work was supported partly by a Grant-in-Aid for Scientific Research on Priority Areas (No. 260) from The Ministry of Education, Science and Culture, and a NEDO International Joint Research Grant.

References

[1] A C.W.P James and J.B. Goodenough, *J Solid State Chem*, *74* (1988) 287–294
[2] P Strobel and B Lambert-Andron, *J Solid State Chem.*, *75* (1988) 90–98.
[3] J.F. Dulac, *CR Acad. Sci. Paris Ser. B*, *270* (1970) 223–226.
[4] M. Jansen and R. Hoppe, *Z Anorg Allg Chem.*, *397* (1973) 279–289.
[5] A. Riou, A Lecerf, Y. Gerault and Y. Cudennec, *Mater. Res Bull*, *27* (1992) 269–275.
[6] J.F. Dorrian and R.E. Newnham, *Mater. Res. Bull.*, *4* (1969) 179–184.
[7] G Von Lang, *Z. Anorg. Allg Chem.*, *348* (1966) 246–256
[8] J L. Hodeau, M Marezio, A. Santoro and R S Roth, *J Solid State Chem.*, *45* (1982) 170–179.
[9] A.C.W.P. James and J.B Goodenough, *J Solid State Chem*, *76* (1988) 87–96.
[10] J. Gopalakrishnan and V Bhat, *Mater. Res Bull*, *22* (1987) 769–774

[11] N. Kumada, S Muramatsu, N. Kinomura and F. Muto, *J. Ceram. Soc Japan*, 96 (1988) 1181–1185.
[12] H. Kobayashi, R Kanno, Y. Kawamoto, M Tabuchi, O Nakamura and M. Takano, *Solid State Ionics*, 82 (1995) 25–31
[13] H. Kobayashi, R. Kanno, Y. Kawamoto, M Tabuchi and O Nakamura, *Solid State Ionics*, in press
[14] R.D. Shannon and C.T. Prewitt, *Acta Crystallogr*, B25 (1969) 925–946.
[15] F Izumi, in R A Young (ed.), *The Rietveld Method*, Oxford University Press, Oxford, 1993, Ch. 13.
[16] M Gadzhiev and I. Shaplygin, *Russ. J Inorg. Chem*, 29 (1944) 1231–1232.